Chapter 11

Homology Model-Assisted Elucidation of Binding Sites in GPCRs

Anat Levit, Dov Barak, Maik Behrens, Wolfgang Meyerhof, and Masha Y. Niv

Abstract

G protein-coupled receptors (GPCRs) are important mediators of cell signaling and a major family of drug targets. Despite recent breakthroughs, experimental elucidation of GPCR structures remains a formidable challenge. Homology modeling of 3D structures of GPCRs provides a practical tool for elucidating the structural determinants governing the interactions of these important receptors with their ligands. The working model of the binding site can then be used for virtual screening of additional ligands that may fit this site, for determining and comparing specificity profiles of related receptors, and for structure-based design of agonists and antagonists. The current review presents the protocol and enumerates the steps for modeling and validating the residues involved in ligand binding. The main stages include (a) modeling the receptor structure using an automated fragment-based approach, (b) predicting potential binding pockets, (c) docking known binders, (d) analyzing predicted interactions and comparing with positions that have been shown to bind ligands in other receptors, (e) validating the structural model by mutagenesis.

Key words: Docking, GPCR model, Binding site, Agonist, Antagonist, Taste receptors, Broad tuning, Receptor range, Molecular recognition

1. Introduction

G protein-coupled receptors (GPCRs) are the largest family of membrane proteins serving as key signal-transduction proteins and representing a major class of drug targets (1). Recent breakthroughs in GPCR crystallography (2–5) provide exciting opportunities for structure-based drug design methods that can now use increasingly reliable homology models of GPCR targets (6, 7). Successful computational models of GPCRs have been used for virtual screening, enriching the rate of ligand hits relative to a random collection of compounds, with hit rates ranging from 3 to 21% (8, 9), comparable to virtual screening success rates with X-ray

Nagarajan Vaidehi and Judith Klein-Seetharaman (eds.), *Membrane Protein Structure and Dynamics: Methods and Protocols*, Methods in Molecular Biology, vol. 914, DOI 10.1007/978-1-62703-023-6_11,

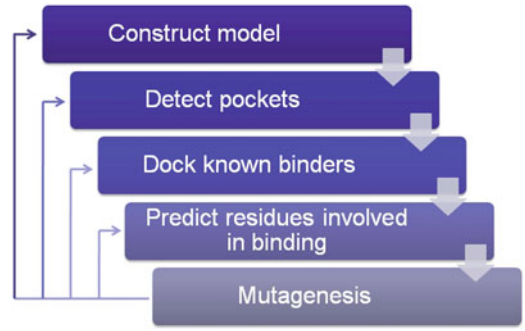

Fig. 1. Scheme of binding-site elucidation procedure.

structures (8). Furthermore, research aimed at elucidating the underlying principles determining the molecular responsiveness range of GPCRs that mediate senses, such as odor (10) and taste (11, 12) receptors, depends on the ability to build reliable models of the interaction sites. A crucial step in understanding specificity and promiscuity in molecular recognition and structure-based design is to identify the residues that are important for ligand binding.

Sequence-based classification systems have been developed to facilitate the analysis of GPCRs, the two most widely used being the *GRAFS* (13) and the UIPHAR (14). The *GRAFS* classifies GPCRs into families: *R*hodopsin (which corresponds to UIPHAR class A), *S*ecretin (UIPHAR class B), *A*dhesion (UIPHAR class B), *G*lutamate (UIPHAR class C), and *F*rizzled/Taste2. While researchers have successfully applied homology-based GPCR structure modeling approaches to ligand-binding elucidation similar to the one described below to understanding the role of modulators in class C (15) and class B GPCRs (9, 16), this review is focused on application of homology-based models primarily to class A (17–19) and Taste2 (T2R) GPCRs (12, 20, 21).

Several approaches to modeling GPCRs have been described (7), including *ab initio* (8, 22) and template based (6, 19, 23). Following previous work (7, 12), here we illustrate the use of a fragment-based approach, using the I-TASSER server (24) for homology modeling of the human bitter-taste receptor hTAS2R46, which belongs to the Frizzled/Taste2 family. The steps toward homology model-assisted elucidation of the binding-site residues discussed in this protocol are described in the flowchart in Fig. 1.

2. Materials

2.1. Sequence of the GPCR Being Studied

The protein sequence of interest may be obtained via NCBI (http://www.ncbi.nlm.nih.gov/protein) or Uniprot (http://www.uniprot.org/) databases, or from the GPCRDB database (http://www.gpcr.org/7tm/).

2.2. Ballesteros–Weinstein Numbering

To facilitate comparisons between different GPCRs, we use Ballesteros–Weinstein (BW) numbering (25), in which the most conserved residue in a given transmembrane (TM) domain X is assigned the index X.50, and the remaining TM residues are numbered relative to this position. For example, the most conserved position in TM6 is designated 6.50.

2.3. A List of Known Binders

To dock ligands into the predicted binding site, a list of ligands that are known to bind or activate (known binders or activators) the receptor is needed. These data may be obtained from the GLIDA database, which provides interaction data between GPCRs and their ligands along with chemical information on the ligands (26), directly from the literature, or experimentally.

2.4. Servers Used for Modeling in This Protocol

Structure modeling: I-TASSER (http://zhanglab.ccmb.med.umich.edu/I-TASSER).

Cavity detection: QSiteFinder (http://www.modelling.leeds.ac.uk/qsitefinder/).

PocketFinder (http://www.modelling.leeds.ac.uk/pocketfinder/).

Cavity detection allows for the identification of nonorthodox and allosteric binding sites (see also (27)).

2.5. Mutation Databases

- TinyGRAP database (28) (http://www.cmbi.ru.nl/tinygrap/search/).
- Some mutations can be extracted using GPCRDB (http://www.gpcr.org/7tm/) or the MuteXt repository of mutations (29).

2.6. Structure-Based Sequence Alignment

TCoffee (http://tcoffee.vital-it.ch/cgi-bin/Tcoffee/tcoffee_cgi/index.cgi).

2.7. Ligand Preparation and Docking

Software

The Discovery Studio 2.5 software package (Accelrys, Inc.) is used in this protocol as follows:

- Generation of Ramachandran plots of the modeled protein to assess its quality by checking the predicted torsion angles.
- Ligand preparation prior to docking experiments, using the "Prepare Ligands" protocol, which removes duplicate structures, enumerates isomers and tautomers, sets standard formal charges on common functional groups, sets ionization states at a given pH range, and generates 3D conformations.
- Docking of small molecule ligands to the receptor. In this protocol we use the "Flexible Docking" option, which allows for some receptor flexibility during docking of flexible ligands. A typical docking simulation of one compound using the "Flexible Docking" module requires 10 min on a Pentium 4,

2 GB RAM, 2.8 GHz dual core computer (for precomputed protein conformations, and program ran with parallel processing).

- Docking pose analysis is performed using the "Analyze ligand poses" protocol. The protocol enables calculation of the RMSD of the poses to each other or to a reference pose, identification of ligand–receptor hydrogen bonds at varying degrees of detail, and analysis of contacts between the ligand and the receptor (including clashes).
- Plotting a ligand–receptor interaction diagram in 2D using the "draw ligand interaction diagram" tool in the "analyze binding site" module.

Hardware

For best performance, the Discovery Studio software should be installed on a server with an Intel-compatible ≥2 GHz processor with x86 or x86_64 architecture, and an SGE 6.1 grid engine. A minimum of 2 GB of memory for Discovery Studio Client and 2 GB for the Pipeline Pilot Server is required. Ideally, a total of 4 GB should be available if the client and server are installed on the same machine.

2.8. Site-Directed Mutagenesis and Functional Assays

The computational process described in this protocol generates a structural model for the GPCR and the ligand binding site that is next validated using site-directed mutagenesis work. The cDNAs spanning the coding region of the receptor of interest should be cloned into a vector that allows expression in eukaryotic cell lines. Oligonucleotides for mutagenesis and vector-specific primers can be ordered online. Thermostable DNA polymerase with proof-reading activity such as *Pfu*-DNA polymerase is preferred. Deoxyribonucleotides (dGTP, dATP, dTTP, and dCTP): prepare a stock solution of, e.g., 2.5 mM each (10 mM total) and store in aliquots at –20°C. There are no specific requirements for the thermocyclers used for the polymerase chain reaction (PCR) amplification.

For agarose gel electrophoresis, use high-quality agarose suitable for DNA-fragment recovery. After gel electrophoresis, the DNA bands of interest are excised from the ethidium bromide-stained gels on a UV-transilluminator (eye protection is necessary!) and purified using a commercially available spin column purification kit. Appropriate restriction endonucleases, T4-DNA ligase, and chemically competent bacterial cells are required for subcloning. For the transfection of eukaryotic cells, use highly purified plasmid DNA of mutated constructs which have been analyzed by DNA sequencing to confirm their integrity.

2.9. Functional Heterologous Expression

We use cells of the human embryonic kidney cell line HEK 293 T stably expressing the G protein chimera Gα16gust44 for functional expression. High-quality fetal bovine serum, Dulbecco's Modified Eagle's Medium (DMEM), and a sterile workbench, as well as incubators providing constant temperature (37°C), humidity, and CO_2 levels (5%), are necessary for cultivation of cells. For materials used in calcium-imaging assays, see Subheading 3.

3. Methods

We illustrate the flowchart in Fig. 1 using the hTAS2R46 example, generally following the steps performed in our recent paper (12):

1. Obtain the sequence of the hTAS2R46 receptor from the Uniprot database (accession no. P59540).
2. Submit to I-TASSER Web site in order to generate a homology model of the protein: go to the I-TASSER Web page (http://zhanglab.ccmb.med.umich.edu/I-TASSER/) and follow these steps:
   (a) Copy-paste the protein sequence onto the provided form or directly upload the sequence from a file.
   (b) Provide an e-mail address where results will be sent upon job completion.
   (c) Provide a name for the protein (optional).
   (d) Specify additional restraints to guide I-TASSER modeling (optional): a file containing contact/distance restraints may be optionally uploaded by the user, as well as specification of the template to be used during the modeling process (this can be achieved by either PDB code specification or by uploading a PDB file, with or without an alignment file; see below).
   (e) The user may also exclude some homologous templates from the I-TASSER template library (optional). This new option is most useful for validation studies, such as testing homology model performance when an experimental structure is available in the database, or when a particular structure is to be excluded from the templates due to its quality, conformational state, or other reasons.
   (f) To submit the sequence for modeling, click the "Run I-TASSER" button. The browser will be directed to an acknowledgment page that will display confirmation of the submitted sequence, a job identification number, restraint information, and a link to the page that will contain the detailed results when the job is complete.

An example of a model generated by I-TASSER for hTAS2R46 is shown in Fig. 2a. This model is based on the (automatically selected) X-ray structures of human β2-adrenergic receptor (β2ADR; PDB code 2RH1), turkey β1-adrenergic receptor (2VT4), human A2A adenosine receptor (3EML), squid rhodopsin (2Z73), and bovine rhodopsin (1l9h).

3. The generated model is validated by examining the Ramachandran plot. Such plots may be generated using a stand-alone modeling software package, such as Discovery Studio 2.5 (Accelrys, Inc.), or by use of different Web servers, such as PROCHECK (http://www.ebi.ac.uk/thornton-srv/software/PROCHECK/). Figure 2b shows a Ramachandran plot generated for the hTAS2R46 model using PROCHECK, where dihedral angles for most residues appear in the core ("allowed") regions of the plot, as expected.
4. Validate the model by comparing the most conserved residue positions in GPCRs named as BW positions with template structures. A structure-based multiple-sequence alignment of the Class A X-ray structures may be obtained by the structure-based sequence alignment option on the TCoffee Web server (http://tcoffee.vital-it.ch/cgi-bin/Tcoffee/tcoffee_cgi/index.cgi); Fig. 3. As expected, the most conserved positions in each TM helix (BW X.50 positions) are in alignment. Next, the model can be aligned to this multiple sequence alignment using the Combine Option on the TCoffee server. All (within

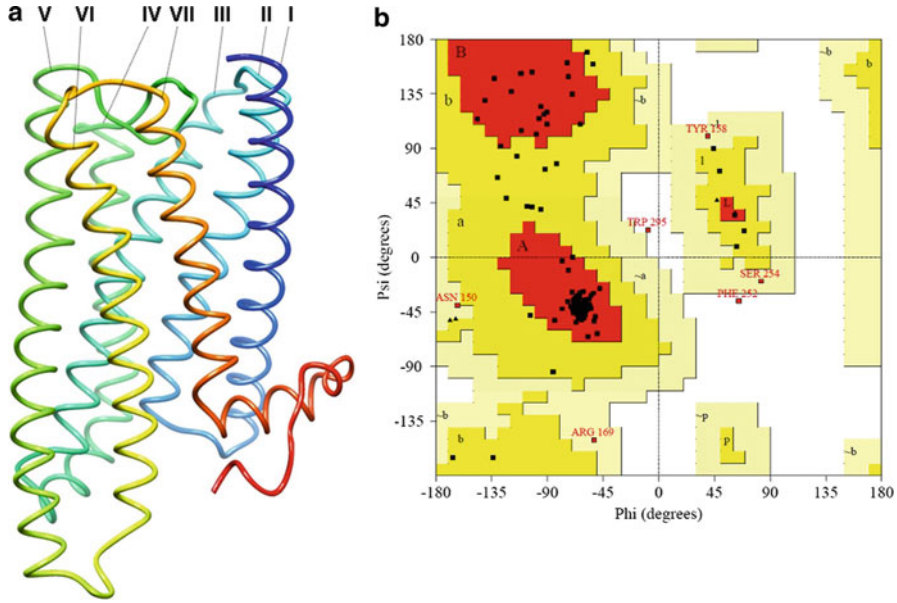

Fig. 2. Model and model quality assessment.

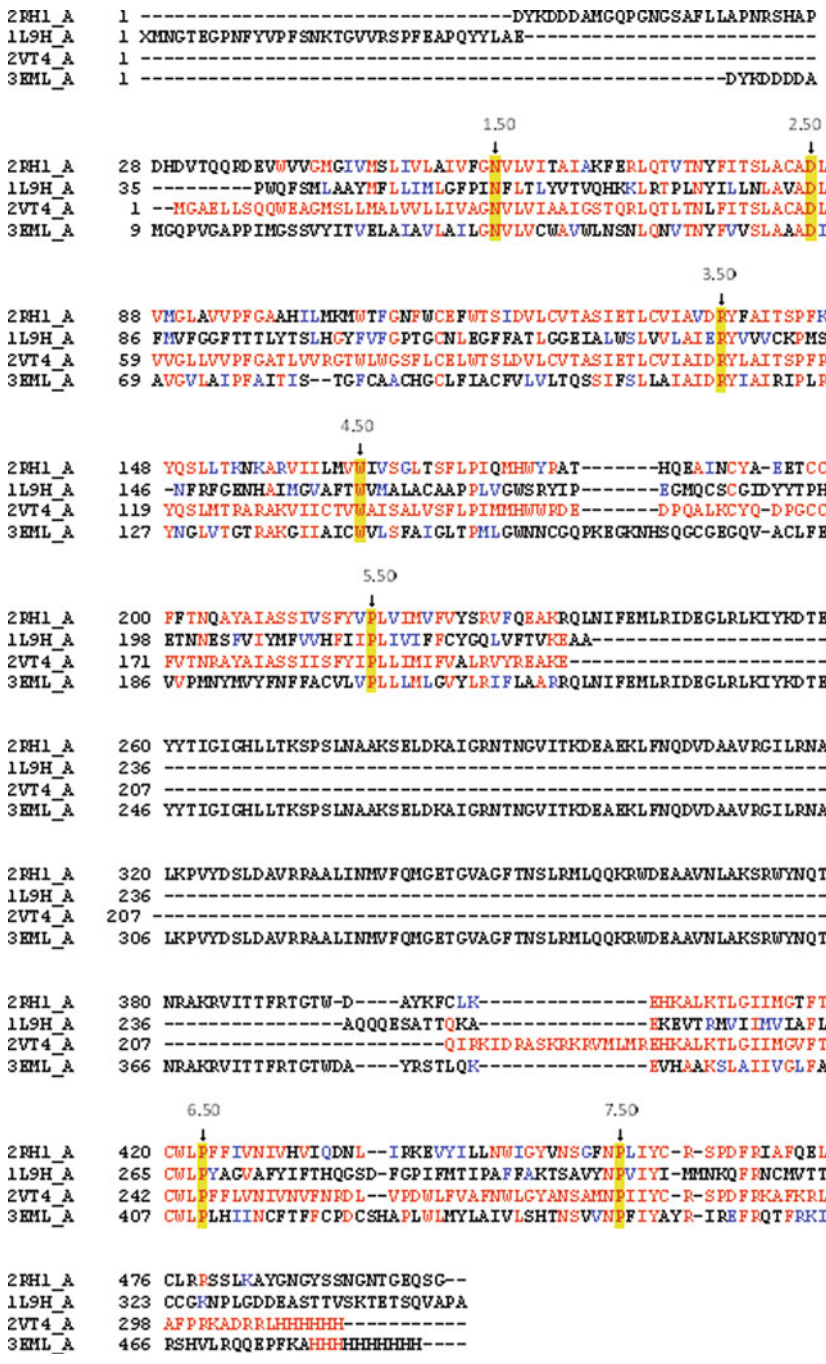

Fig. 3. Structure-based multiple-sequence alignment and BW numbering.

Class A) or several (in other classes) BW positions are expected to align in a correct model. For the Frizzled/Taste 2 receptor hTAS2R46 model the aligned positions include N21$^{1.50}$, P187$^{5.50}$, and P276$^{7.50}$.

5. Loop deletion: Modeling of loops remains one of the greatest challenges in modeling GPCRs due to their length and receptor-to-receptor variability. Several studies have shown that unless the models are based on a closely related template (e.g., β2ADR and β1ADR) (6, 30, 31), models without loops are preferable for use in docking studies. In particular, deletion of the second extracellular loop (ECL2) ((7) and see Note 1) is recommended. ECL2 is defined as the loop connecting TM4 and TM5, residues N150 to R169 in the case of hTAS2R46. The model may be structurally aligned to its X-ray templates to facilitate identification of loop boundaries.
6. Predict the binding pockets: Prediction of the putative ligand-binding pockets within the TM bundle is performed using the QSiteFinder Web server (32), which uses the interaction energy between the protein and a van der Waals methyl probe ($-CH_3$) to locate energetically favorable binding sites, and is especially useful for detection of relatively small sites. Protein residues within 5 Å of each predicted binding site are identified as potentially contacting residues. To validate QSiteFinder performance for GPCRs, we submitted the β2ADR structure (with antagonist deleted; PDB code 2RH1) and found that the predicted antagonist and cholesterol-binding pockets were in good agreement with the published experimentally determined structures (PDB codes 2RH1, 3D4S; data not shown) (33, 34). For hTAS2R46, the server predicted several different sites, of which we chose to further analyze the top binding-site clusters. As shown in Fig. 4, the largest and most energetically favorable binding site is predicted to be located between TM3 and TM7, in agreement with previous work on a related bitter-taste receptor (35, 36): most data for GPCRs in general point toward the same pocket as being the binding site for multiple ligands of many GPCRs (see Note 2). The importance of some positions (such as 3.32, 7.39—BW numbering) was illustrated for a wide range of receptors (see Note 2), but differences between related receptors in the roles of the residues within the main binding site were also shown (see Note 3). For some receptors only subtle changes occur in agonist bound vs. antagonist conformations (4, 37) but may be more pronounced in other receptors, as the A_{2A} adenosine receptor agonist-bound structure indicates (5). In the latter case, models based on an inactive state crystal structure may not be optimal as pockets for docking of agonists (see Note 4).
7. Check for known mutations using mutational databases such as GPCRDB (http://www.gpcr.org/7tm/) and tinyGRAP (http://www.cmbi.ru.nl/tinygrap/). Such mutations may provide supporting evidence for residues predicted in step 6 to be involved in ligand binding (28, 38). On the GPCRDB

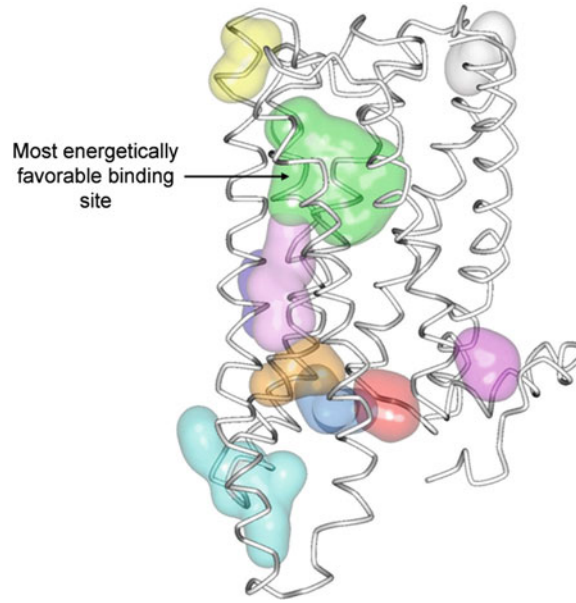

Fig. 4. QSiteFinder mapping of the hTAS2R46 model binding sites.

home page, choose the browse option (by families). Choose the appropriate GPCR family from the hierarchy view, and follow the "open alignment" link in the "alignment" field that appears following selection of the GPCR family. Select the JalView option for visualization of mutational data on the alignment. The known mutated positions are indicated in white font. Each such position is linked to an annotation of the mutation, including the amino acid to which the position was mutated, BW notation, TM domain, and links to the relevant literature. For the case of hTAS2R46, we did not find mutational data in these databases.

8. Dock a known ligand into the binding pocket of choice. In our working example, following Brockhoff et al. (12), we docked strychnine (a known ligand of the receptor) into the most energetically favorable binding site. We use the "Flexible Docking" algorithm as implemented in Discovery Studio 2.5 (Accelrys, Inc.). Additional docking algorithms, such as GOLD (39), GLIDE (40, 41), LigandFit (42), and CDocker (43), have also been successfully used, as reported in the literature. For a comprehensive recent review see Senderowitz et al. (8). Prior to docking, the ligands should be carefully prepared so that they are good representations of the actual ligand structures that would appear in a protein–ligand complex. The following is a "checklist" for ligand preparation:

   (a) A 3D structure of the ligand is needed, without any accompanying fragments such as counterions and solvent molecules.

The most stable, or preferably a number of, 3D conformations should be used for docking.

(b) The bond lengths and bond angles are appropriate.

(c) The ligand has all the hydrogens added (filled valances).

(d) The ligand is in its appropriate protonation state for physiological pH values (~7). Inappropriate protonation states may, for example, result in docking of a polar molecule into a hydrophobic region, or cause it to serve as a hydrogen bond acceptor.

(e) Generate tautomers, alternative chiralities, and low-energy ring conformations, where applicable.
Steps (a–e) may be facilitated by using "LigPrep" (Schrödinger, Inc.) software, a recommended option for ligand preparation.

9. After docking, and according to the obtained poses, identify residues that are involved in ligand binding and suggest mutagenesis. Poses generated in the docking experiments are clustered, e.g., by means of root mean square deviation (RMSD) of all poses from the top scoring pose (using "analyze ligand poses" protocol, Discovery Studio 2.5, Accelrys, Inc.). Several distinct poses are chosen for further examination, which includes identification of all residues within 5 Å of the docked ligand, and determination of specific ligand–receptor contacts, such as hydrogen bonds and π–π and π–cation interactions. The latter may also be achieved by generation of ligand plots—2D representations of all ligand-contacting residues, e.g., using LigPlot (44). Residues are then chosen for experimental validation by site-directed mutagenesis, followed by binding/activity assays. The candidate residues are chosen based on their chemical nature, distance, and orientation from the ligand. In addition, it is important to test those positions which discriminate between two distinct ligand poses (for example, occupying two separate regions in the same cavity). For hTAS2R46, such residues include $W88^{3.32}$, $A89^{3.33}$, $N92^{3.36}$, $H93^{3.37}$, $N96^{3.40}$, $I245^{6.55}$, $E265^{7.39}$, and $A268^{7.42}$ (see Fig. 5 for one example of a chosen pose and surrounding residues). Variations in binding residues for different ligands (even of the same pharmacology) are not uncommon (see Note 5).

3.1. In Vitro Mutagenesis

Site-directed mutagenesis can be performed by various methods which rely on the exchange of nucleotides within the coding sequence of the target receptor by way of synthetic oligonucleotides. We typically perform site-directed mutagenesis by PCR-mediated recombination, a method originally described by Fang and colleagues (45). This versatile method is not restricted to the

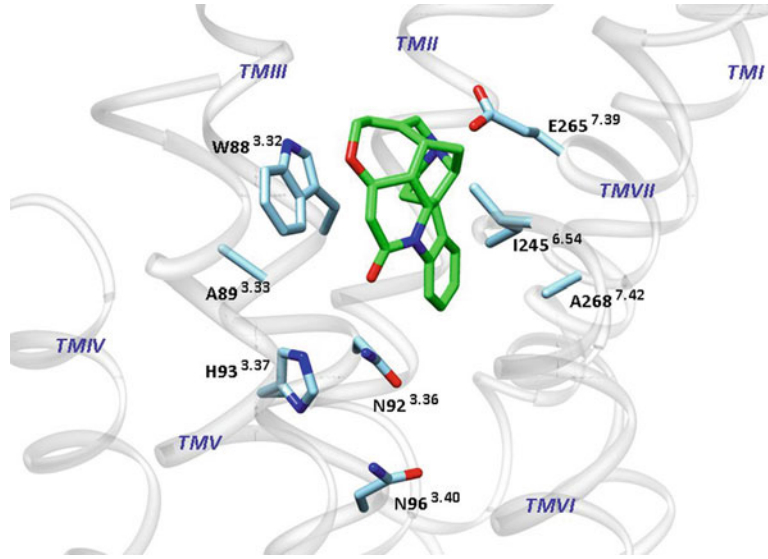

Fig. 5. Strychnine docked into the proposed binding pocket of hTAS2R46.

mutagenesis of one to several nucleotides in the context of an existing double-stranded DNA template (46); it is also useful, as originally intended, to generate chimeric receptor constructs (12) or other major modifications, such as the introduction of epitope tags (47). For successful point mutagenesis, design of synthetic oligonucleotides is crucial. Numerous companies offer rather inexpensive custom oligonucleotide syntheses with rapid turnaround via the Internet. The nucleotide sequence to be modified should be located in the center of a complementary primer pair and flanked by a sufficient number of nucleotides that are an exact match to the sequence of the DNA template to allow efficient annealing during the subsequent PCR. Depending upon the context of the codon(s) being subjected to mutagenesis, oligonucleotides of 21–30 bases are usually sufficient. For a schematic overview of the PCR steps involved in this procedure see Fig. 6.

In the first step, each of the two complementary oligonucleotides is used in combination with a primer specific for upstream and downstream vector sequences, respectively, to produce two subfragments corresponding to the 5′ and 3′ parts of the mutated cDNA (Fig. 6b). When calculating the annealing temperature, it is important to take the number of mismatches between primer and template sequences into account. A reduction of the annealing temperature by 1–1.5°C per percent mismatch is usually sufficient for efficient amplification. The annealing temperature prior to mismatch correction is 3–5°C below the calculated melting temperature, which is generally provided by the company on the

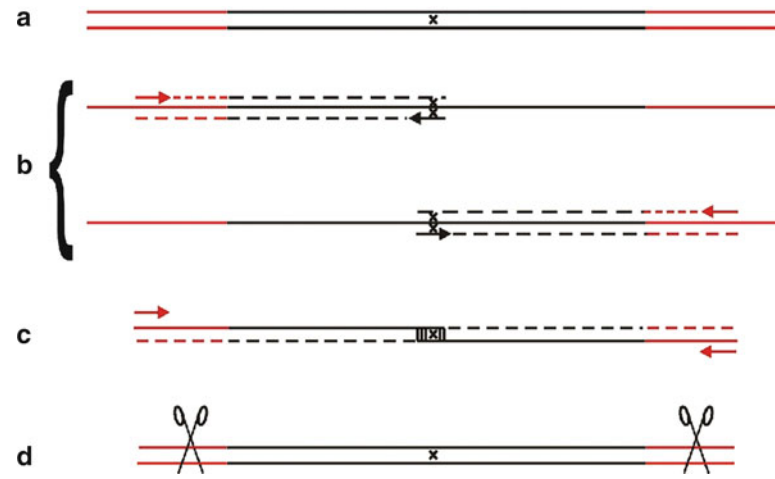

Fig. 6. *In vitro* mutagenesis flowchart.

accompanying data sheet assigned for oligonucleotide synthesis. An example procedure is described below.

PCR sample:

*X*µL Template DNA (~10 ng)
0.5 µL Forward/reverse mutagenesis primer (10 µM)
0.5 µL Reverse/forward vector primer (10 µM)
2.5 µL 10× *Pfu*-DNA-polymerase buffer (including magnesium)
2.0 µL dNTP-mixture (2.5 mM each)
1.0 µL *Pfu*-DNA polymerase (3 U/µL)
Add 25 µL deionized H_2O

PCR conditions:

1. 5 min 95°C Denaturation (perform "hot-start" during this time)
2. 1 min *X*°C annealing
3. 2 min 72°C Polymerization (~2 min/1 kb; check with supplier of DNA polymerase for optimal temperature)
4. 0.5 min 95°C
5. 5 min *X*°C Annealing
6. 10 min 72°C Polymerization

Repeat steps (2–5) 15–20 times (alternatively, after 3–5 initial PCR cycles, you may want to increase the annealing temperature for the remaining cycles as the mutagenesis primers are already incorporated).

After purification of the subfragments from non-incorporated mutagenesis primers and traces of the original template DNA by, e.g., isolating the PCR products from agarose gels, the subfragments are mixed in approximately equimolar amounts and further amplified

by PCR using the pair of vector-specific primers (Fig. 6c). If the annealing temperature of the vector-specific primers exceeds the annealing temperature of the mutagenesis primers, which now form the overlap between the subfragments, at least 3–5 PCR cycles at the beginning of the amplification must be performed at a lower annealing temperature. However, a mismatch between the original template DNA and the mutated sequence does not need to be taken into account, as the mutation is already incorporated. A typical recombinant PCR step is shown below:

PCR sample:

0.5 µL Subfragment A (~5 ng)
0.5 µL Subfragment B (~5 ng)
0.5 µL Forward vector primer (10 µM)
0.5 µL Reverse vector primer (10 µM)
2.5 µL 10× *Pfu*-DNA-polymerase buffer (including magnesium)
2.0 µL dNTP mixture (2.5 mM each)
1.0 µL *Pfu*-DNA polymerase (3 U/µL)
Add 25 µL Deionized H_2O

PCR conditions:

1. 5 min 95°C Denaturation (perform "hot-start" during this time)
2. 1 min *X*°C Annealing
3. 2 min 72°C Polymerization (~2 min/1 kb; check with supplier of DNA polymerase for optimal temperature)
4. 0.5 min 95°C
5. 5 min *X*°C Annealing
6. 10 min 72°C Polymerization

Repeat steps (2–5) 15–20 times (if optimal annealing temperature of overlapping sequence between subfragments A and B is lower than the annealing temperature of the vector primers, perform 3–5 initial PCR cycles at an annealing temperature specific for the overlap and increase the annealing temperature for the remaining cycles).

The use of thermostable DNA polymerases with proofreading function is advisable for the described PCRs to avoid the accumulation of PCR products containing additional, unwanted mutations. Since vector-specific primers are used for the generation of mutated cDNAs, the PCR products contain the multiple-cloning site that enables, after purification and restriction-endonuclease treatment, reintroduction into the same vector (Fig. 6d). After the integrity of the constructs is confirmed by sequencing, the mutated construct can be subjected to functional characterization.

If no particular type of interaction involving the amino acid in question has been predicted by computer modeling, an exchange to alanine ("alanine-scanning mutagenesis" (48)) can be performed as an initial step.

3.2. Functional Heterologous Expression Assays

In our lab, functional characterization of receptor mutants is performed using HEK 293T cells stably expressing the G-protein chimera Gα16gust44. The G-protein chimera consists of Gα16, which couples, upon activation, to the IP_3/calcium second messenger-signaling pathway, and the last 44 amino acids of α-gustducin for effective interaction with T2R proteins (49). For the characterization of receptor mutants, it is important to include the parental receptor(s) and an empty cloning vector (mock control) for transient transfection. The cells are seeded onto black 96-well plates with clear bottom and transfected using Lipofectamine 2000 reagent (Invitrogen) at a cell density of ~60–70%. After ~24 h, the cells are loaded with the membrane-permeable calcium-sensitive dye, Fluo4-am, for 1 h in the presence of probenicid, an agent that inhibits the organic anion-transporter type 1, thus preventing rapid extrusion of the dye (50). While working with this or related fluorescent dyes, prolonged exposure of samples to bright light should be avoided. Now the cells are washed three times with buffer (130 mM NaCl, 5 mM KCl, 2 mM $CaCl_2$, 10 mM glucose, 10 mM HEPES, pH 7.4) using an automated microtiter plate washer to remove excess dye. After each washing step, the cells are incubated for ~15 min in 100 µL buffer. Next, the plates are transferred to a fluorometric imaging plate reader (FLIPR, Molecular Devices) and the baseline fluorescence is monitored. After application of an appropriate agonist concentration series, e.g., 0.003–100 µM strychnine for the hTAS2R46 (threefold concentrated in 50 µL applied to 100 µL present in each well), changes in fluorescence are recorded until the peaks of agonist-induced fluorescence are evident. After the signal has returned to baseline, a second application of an agonist stimulating transient calcium release from intracellular stores via an endogenous receptor is recommended to check cell viability (e.g., 100 nM somatostatin-14 stimulating endogenous somatostatin receptor, or 1 µM isoproterenol to activate β-adrenergic receptors. Note that these agonists have to be applied at fourfold concentration, if 50 µL are applied: a 100-µL volume is placed initially in each well, and then 50 µL of agonist solution is added; the total is 150 µL, so a threefold-concentrated agonist solution is needed. Addition of another 50 µL leads to 200 µL total volume, so the agonist concentration should be fourfold). For calculation of dose–response relations, at least two independent experiments with triplicate measurements of each construct and agonist concentration should be performed. Fluorescence changes of mock-transfected cells are subtracted and signals are normalized to background fluorescence. Calculations of EC_{50} concentrations by nonlinear regression of the plots to the function $f(x) = 100/[(EC_{50}/x)^{nH}]$ and generation of the corresponding graphics are performed using Sigma Plot (for more details on the functional assay procedure see, e.g., (51–53)).

3.3. Interpretation of the Results

This can be a rather challenging task. The mutated receptor may deviate from the parental wild-type receptor by its EC_{50} value, threshold concentration, maximal amplitude of the fluorescence signal, or a combination of these parameters. Furthermore, mutants of receptors with multiple agonists, such as many human bitter-taste receptors, may show the aforementioned changes in their dose–response curves for single, multiple, or all agonists. An idealized example of dose–response relationships is depicted in Fig. 7.

Clearly, a pure shift in the EC_{50} value indicates a change in agonist interaction that can be fully compensated for by the application of different agonist concentrations (Fig. 7, curve b). On the contrary, if the EC_{50} concentration remains unaffected but the maximal amplitude has changed, the amino-acid exchange apparently affected receptor activation capability rather than agonist interaction (Fig. 7, curve c). The most difficult outcome, however, is loss of function of the mutant receptor (see Note 6).

Note also that not in all cases where mutation of a residue affects agonist-induced response, a direct contact exists (see Note 7). The effect of mutation on ligand may be due to an allosteric effect as well. Nevertheless, in the few cases in which validation using X-ray structure was possible, the results were encouraging (see Note 8). Furthermore, many successful virtual-screening campaigns have provided confirmation of binding-site models derived as described above (9, 54).

Using the above procedure, residues located close to the docked strychnine molecule (see Fig. 5) were mutated. We show the results for some positions in Table 1, in which the mutations were designed to exchange residues of the strychnine-activated hTAS2R46 for residues of hTAS2R31, a bitter-taste receptor which is not activated by strychnine (12). Indeed the mutations led to a decrease in receptor responsiveness upon stimulation with the

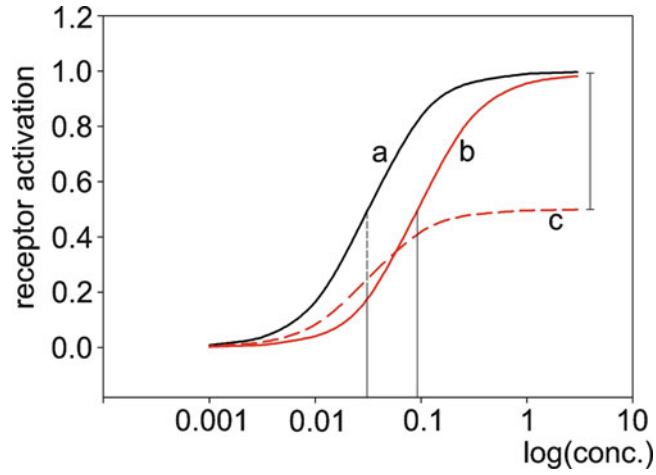

Fig. 7. Idealized dose–response curves of receptor mutants.

Table 1
hTAS2R46 binding-site residues

Mutation	Effect
hTAS2R46 wild type	Threshold ~ 0.1 μM[a]
$N92G^{3.36}$	Nd. Strong decrease in responsiveness[b]
$E265K^{7.39}$	Threshold ~ 30 μM[b]
$A268R^{7.42}$	Threshold ~ 30 μM[b]

Mutagenesis of hTAS2R46 amino-acid residues located close to the docked strychnine molecule. All mutations were designed to cause an exchange of hTAS2R46 residues with hTAS2R31 residues. Threshold values were taken from (55) ([a]) and (12) ([b]). Note that all mutations led to severe decreases in receptor responses upon stimulation with the hTAS2R46 agonist strychnine and hence determination of EC_{50} values was not possible. *Nd.* not determined.

hTAS2R46 agonist strychnine. Interestingly, the double mutation of E265K and A268R exhibited loss of function for strychnine and gain of function for the hTAS2R31-specific agonist aristolochic acid (12).

4. Notes

1. Using GPCR models without loops

   The role of GPCR extracellular loops in binding high-molecular-weight peptidic ligands is well established (56). Studies have demonstrated that the extracellular loops, specifically ECL2, also interact with low-molecular-weight ligands, such as biogenic amines or adenosines (57). The recently reported X-ray structures of various GPCRs demonstrate that these extracellular loops also differ greatly in their structural features (3, 58). Furthermore, nuclear magnetic resonance (NMR) studies have revealed the dynamic and ligand-dependent characteristics of ECL2 in β2ADR (59), and the activation-induced and TM5-coupled changes in the rhodopsin ECL2 (60). The accurate modeling of these loops is therefore far from trivial.

   The available approaches to loop treatment, namely, homology modeling, use of loopless models, and *de novo* prediction, are summarized in our recent review (7). The emerging consensus is that models perform better with no modeled loops at all than with badly modeled loops, and that *de novo* modeling approaches warrant further development.

2. Comparison of known binding-site residues in different GPCRs

   Experimental data from Shi and Javitch (61) and de Graaf and Rognan (9) reviews and from recent papers (12, 19–21, 62–69) on residues corresponding to the upper inside part of the TM bundle in solved GPCR structures ((70), and current work) show that they are involved in ligand binding. The residues are shown in Table 2 and listed in Fig. 8.

3. Variation in binding orientation between different receptors

   The adenosine receptor 2A X-ray structure (3EML) revealed that the antagonist is positioned higher in the binding cavity than in other structures (74). Recent studies of taste receptors have also revealed different effects of mutations in conserved binding-site residues of different receptors. For example, mutation $W^{3.32}A$ in the hTAS2R38 receptor barely affected binding of the agonist (21), while the same mutation in hTAS2R43 and hTAS2R47 (63) had a pronounced effect on agonist-induced activation. This effect depends on the compound that was used to test binding sensitivity (see Note 4). Overall, while particular residues are shown to be involved in the binding of several ligands in several receptors (see Table 2), effects of mutations may also be ligand specific, indicating binding of different ligands in different subareas and orientations within the same pocket.

4. Variation between agonists and antagonists and use of inactive structures for docking agonists

   Virtual screening studies show that *agonists* can be retrieved by using receptor models based on inactive crystal structure templates and, conversely, *antagonists* have been found using *agonist*-based receptor models (see (9) and references therein). However, active structure properties inferred from indirect measurements, as summarized, e.g., in (17), and directly from X-ray structures (4, 5, 75) indicate significant differences from the inactive form. The recent structural data indicates that the degree of variation in the agonist-bound vs. antagonist-bound pockets is receptor dependent.

   Strategies for accommodating changes in the binding site include *in silico* activation (76) and agonist-induced modeling, as recently reviewed (7, 77). Other methods use advanced free-energy mapping methods to study activation dynamics and intermediate-state stabilization by ligands (78, 79). The new experimental structures now also enable inclusion of active structures (PDB codes: 3CAP, 3P0G, 3QAK) as templates for modeling (e.g., ligand-free native opsin structure (3CAP) was recently used (21, 80)).

5. Ligand-specific binding in the same receptor (a residue that is important for one ligand may not be important for another)

Table 2
Summary of binding-site residues

Position	Receptor	Inferred role	Reference	Residue number in human β2ADR
1.35	Adenosine A_{2A}	Water-mediated agonist contact (X-ray)	(5)	M36
2.60	CXCR4	Antagonist contact (X-ray)	(71)	F89
2.61	β1ADR	Ligand-specific partial agonist contact (X-ray)	(72)	G90
	Adenosine A_{2A}	Water-mediated agonist contact (X-ray)	(5)	
	D3R	Antagonist contact (X-ray)	(73)	
2.63	CXCR4	Antagonist contact (X-ray)	(71)	A92
2.64	Adrenergic	Antagonist specificity	(61)	H93
	β1ADR	Ligand-specific partial agonist contact (X-ray)	(72)	
2.65	β1ADR	Ligand-specific partial agonist contact (X-ray)	(72)	I94
	Taste T2R	Agonist specificity	(12)	
3.25	Muscarinic M1	Interaction with ligand	(68)	C106
3.28	Bioamine receptors	Agonist binding	(69)	F108
	β1ADR	Ligand contact (X-ray)	(72)	
	β2ADR	Ligand contact (X-ray)	(37)	
	D3R	Antagonist contact (X-ray)	(73)	
	CXCR4	Antagonist contact (X-ray)	(71)	
3.29	Muscarinic M1	Interaction with ligand	(68)	W109
	β1ADR	Ligand contact (X-ray)	(72)	
3.32	Dopamine, serotonin, histamine	Interaction with ligand	(61)	D113
	Acetylcholine, adrenergic	Interaction with ligand	(61)	
	CCR5 chemokine	Antagonist binding	(65)	
	Adenosine A_{2A}	Interaction with ligand (X-ray)	(5, 19)	
	Taste T2R	Agonist-induced activation	(12)	
	Taste T2R	Agonist-induced activation	(63)	
	β1ADR	Ligand contact (X-ray)	(72)	
	β2ADR	Ligand contact (X-ray)	(37, 66)	
	D3R	Antagonist contact (X-ray)	(73)	
	CXCR4	Antagonist contact (X-ray)	(71)	
3.33	CCR2 chemokine	Antagonist binding	(65)	V114
	β1ADR	Ligand contact (X-ray)	(72)	
	β2ADR	Inverse agonist-specific contact (X-ray)	(37)	
	Adenosine A_{2A}	Interaction with ligand (X-ray)	(5, 67)	
	D3R	Antagonist contact (X-ray)	(73)	
	Muscarinic M1	Interaction with ligand	(68)	

(continued)

Table 2 (continued)

Position	Receptor	Inferred role	Reference	Residue number in human β2ADR
3.36	Some aminergic receptors	Interaction with some ligands	(61)	V117
	Muscarinic M1	Agonist binding	(68)	
	Bioamine receptors	Agonist binding	(69)	
	β1ADR	Ligand contact (X-ray)	(72)	
	β2ADR	Ligand contact (X-ray)	(37)	
	D3R	Antagonist contact (X-ray)	(73)	
	Adenosine A_{2A}	Agonist contact (X-ray)	(5, 19)	
3.37	Muscarinic M1	Interaction with ligand	(68)	T118
	Adenosine A_{2A}	Interaction with ligand	(19)	
	β2ADR	Inverse agonist-specific contact (X-ray)	(37)	
	Taste T2R	Agonist-induced activation	(21)	
3.40	Histamine	Antagonist specificity	(61)	I121
4.53	Muscarinic M1	Interaction with ligand	(68)	S161
4.57	Muscarinic M1	Interaction with ligand	(68)	T164
4.61	Muscarinic M1	Interaction with ligand	(68)	P168
	Taste T2R	Agonist binding and activation	(64)	
5.29	Adenosine A_{2A}	Antagonist contact (X-ray)	(67)	C190
5.30	Adenosine A_{2A}	Antagonist contact (X-ray)	(67)	C191
5.32	β2ADR	Ligand contact (X-ray)	(37)	F193
5.38	β2ADR	Inverse agonist-specific contact (X-ray)	(37)	Y199
	Adenosine A_{2A}	Ligand contact (X-ray)	(5, 67)	
5.39	β1ADR	Ligand contact (X-ray)	(72)	A200
	β2ADR	Ligand contact (X-ray)	(37)	
	D3R	Antagonist contact (X-ray)	(73)	
	Histamine	Interaction with ligand	(61)	
	Muscarinic M1	Agonist binding	(68)	
5.42	Adrenergic	Interaction with ligand	(61)	S203
	β1ADR	Ligand contact (X-ray)	(72)	
	β2ADR	Ligand contact (X-ray)	(37, 66)	
	D3R	Antagonist contact (X-ray)	(73)	
	Muscarinic M1	Agonist binding	(68)	
	Bioamine receptors	Agonist binding	(69)	
	Adenosine A_{2A}	Antagonist contact (X-ray)	(19, 67)	

(continued)

Table 2 (continued)

Position	Receptor	Inferred role	Reference	Residue number in human β2ADR
5.43	Adrenergic	Interaction with ligand	(61)	S204
	Adenosine A_{2A}	Interaction with ligand	(19)	
	β1ADR	Ligand-specific partial agonist contact (X-ray)	(72)	
	β2ADR	Ligand contact (X-ray)	(37)	
	D3R	Antagonist contact (X-ray)	(73)	
	Taste T2R	Agonist binding and activation	(64)	
5.46	Adrenergic	Interaction with ligand	(61)	S207
	β1ADR	Agonist-specific hydrogen bond (X-ray)	(72)	
	β2ADR	Ligand contact (X-ray)	(37, 66)	
	D3R	Antagonist contact (X-ray)	(73)	
	Muscarinic M1	Agonist binding	(68)	
5.47	Muscarinic M1	Antagonist binding	(68)	F208
6.48	Many aminergic receptors	Ligand binding or activation	(61)	W286
	Muscarinic M1	Interaction with ligand	(68)	
	β1ADR	Antagonist-specific contact (X-ray)	(72)	
	β2ADR	Inverse agonist-specific contact (X-ray)	(37)	
	D3R	Antagonist contact (X-ray)	(73)	
	Adenosine A_{2A}	Interaction with ligand (X-ray)	(5, 67)	
6.51	Many aminergic receptors	Ligand binding or activation	(61)	F289
	Taste T2R	Agonist binding and activation	(64)	
	β1ADR	Ligand contact (X-ray)	(72)	
	β2ADR	Ligand contact (X-ray)	(37)	
	D3R	Antagonist contact (X-ray)	(73)	
	Adenosine A_{2A}	Interaction with ligand (X-ray)	(5, 67)	
	Muscarinic M1	Interaction with ligand	(68)	
	Taste T2R	Agonist-induced activation	(12)	P288
6.52	Many aminergic receptors	Ligand binding or activation	(61)	F290
	Muscarinic M1	Interaction with ligand	(68)	
	β1ADR	Ligand contact (X-ray)	(72)	
	β2ADR	Ligand contact (X-ray)	(37)	
	D3R	Antagonist contact (X-ray)	(73)	
	Adenosine A_{2A}	Agonist contact (X-ray), water-mediated antagonist contact (X-ray)	(5, 67)	

(continued)

Table 2
(continued)

Position	Receptor	Inferred role	Reference	Residue number in human β2ADR
6.55	Adrenergic	Ligand specificity	(61)	N293
	Muscarinic M1	Interaction with ligand	(68)	
	β1ADR	Ligand contact (X-ray)	(72)	
	β2ADR	Ligand contact (X-ray)	(37, 66)	
	D3R	Antagonist contact (X-ray)	(73)	
	Adenosine A_{2A}	Interaction with ligand (X-ray)	(5, 67)	
6.56	D3R	Antagonist contact (X-ray)	(73)	I294
6.58	GnRH	Agonist binding	(62)	H296
6.59	Adenosine A_{2A}	Interaction with ligand	(19)	V297
7.32	Adenosine A_{2A}	Antagonist contact (X-ray)	(67)	K305
7.35	Adrenergic	Agonist selectivity	(61)	Y308
	β1ADR	Ligand-specific full agonist contact (X-ray)	(72)	
	β2ADR	Ligand contact (X-ray)	(37, 66)	
	D3R	Antagonist contact (X-ray)	(73)	
	Adenosine A_{2A}	Interaction with ligand (X-ray)	(5, 67)	
7.36	β1ADR	Full and partial agonist contact (X-ray)	(72)	I309
	β2ADR	Agonist-specific contact (X-ray)	(37)	
	Adenosine A_{2A}	Interaction with ligand (X-ray)	(5, 67)	
7.39	Adrenergic	Ligand specificity	(61)	N312
	Chemokine	Ligand-specific binding	(65)	
	Taste T2R	Antagonist binding	(20)	
	Taste T2R	Agonist specificity (with 7.42)	(12)	
	β1ADR	Ligand contact (X-ray)	(72)	
	β2ADR	Ligand contact (X-ray)	(37, 66)	
	D3R	Antagonist contact (X-ray)	(73)	
	CXCR4	Antagonist contact (X-ray)	(71)	
	Muscarinic M1	Interaction with ligand	(68)	
	Adenosine A_{2A}	Interaction with ligand (X-ray)	(5, 67)	
7.40	β1ADR	Ligand-specific partial agonist contact (X-ray)	(72)	W313
7.42	Taste T2R	Antagonist binding	(20)	G315
	Taste T2R	Agonist specificity (with 7.39)	(12)	
	Adenosine A_{2A}	Agonist specificity	(5, 19)	
	Muscarinic M1	Interaction with ligand	(68)	

(continued)

Table 2 (continued)

Position	Receptor	Inferred role	Reference	Residue number in human β2ADR
7.43	β1ADR	Ligand contact (X-ray)	(72)	Y316
	β2ADR	Ligand contact (X-ray)	(37, 66)	
	D3R	Antagonist contact (X-ray)	(73)	
	Muscarinic M1	Interaction with ligand	(68)	
	Adenosine A_{2A}	Interaction with ligand (X-ray)	(5)	
7.46	Adenosine A_{2A}	Interaction with ligand	(19)	S319
7.49	β2ADR	Antagonist binding	(9)	N322

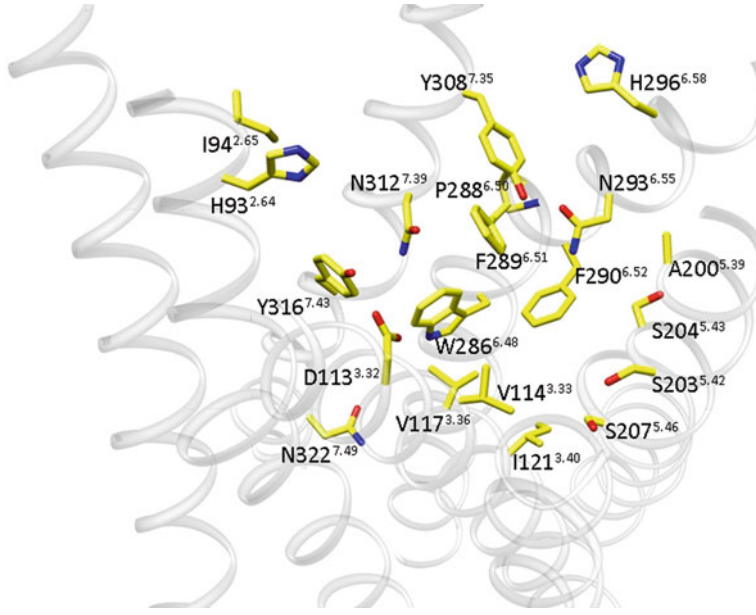

Fig. 8. Visualization of the β2 residues corresponding to experimental data detailed in Table 2.

has been shown (64, 81), as well as in a recent X-ray study of β2ADRs (66). Thus, involvement of a residue in the binding of one ligand does not necessarily imply that it is involved in the binding of another. This is true not only for agonist vs. antagonist, but also for ligands with the same pharmacological effect.

6. Lack of activation in a mutant receptor can be due to a variety of reasons, such as steric hindrance of agonist binding/receptor activation or loss of a crucial agonist interaction site, but it can also be due to receptor misfolding and other complications

in the biosynthetic pathway of the mutated receptor. Immunocytochemical experiments can give some indication of whether such nonspecific event, leading to loss of function, has taken place. If specific antibodies are available or the receptor has been tagged with an epitope, cells can be transiently transfected with receptor constructs and subjected to immunocytochemical analysis. Since GPCRs must reach the plasma membrane to be activated, additional staining with an appropriate cell-surface marker, such as concanavalin A, is strongly recommended. By comparing the staining patterns of the mutant receptor and the corresponding functional wild-type receptor, gross changes in plasma membrane association, and apparent differences in expression levels and intracellular accumulation can be monitored. Nevertheless, conclusive evidence for the proper folding of a nonfunctional receptor is extremely difficult to obtain. An elegant way of addressing this problem is to assemble all those amino-acid residues shown to interact with the agonist in a receptor with a different set of agonists to generate a receptor mutant exhibiting gain of function for the original agonist. However, as this requires the availability of a reasonably closely related, yet pharmacologically distinct, receptor, this approach may not be feasible in all cases.

7. Site-directed mutagenesis effects are observed despite a lack of actual ligand–receptor contact

   In some cases, mutation of a residue affected binding affinity or activation by the ligand, but when the structure was solved, it showed no direct contact. For example (taken from (9)), $V^{3.32}$, $F^{5.43}$, and $H^{7.43}$, which are indicated by site-directed mutagenesis data to be involved in antagonist binding (82, 83), are in fact not in close contact with ZM241385 in the A_{2A} adenosine receptor crystal structure (PDB: 3EML). $D^{2.50}$ in the aminergic receptor, whose mutation reduces affinity for agonists but not for antagonists, is relatively far from the binding site and is likely to influence activation and modulatory effects of sodium on activation (61). Naturally occurring (35, 36) and engineered (21) variations in hTAS2R38 affect its activation even when it is not predicted to be in the binding site. A thermally stable variant of β1ADR carries mutations in residues which are not part of the agonist-binding pocket, but stabilize the inactive state, thus shifting the equilibrium away from the active state (84). This is in line with the ensemble view of allostery in which a certain constituent of the conformational assembly is biologically active (e.g., in signal transduction) and the overall activity is related to the relative occupancy of this conformational state. The occupancy of any conformational state is determined by the differential stability of that state with respect to the overall conformational

distribution and is therefore amenable to modification by mutations that change the conformational distribution (85).

A recent study used advanced sequence analysis and residue swapping to unravel specificity determinants in serotonin and dopamine receptors. Interestingly, the four residue swaps giving the largest enhancement of serotonin responsiveness, I48T$^{1.46}$, M117F$^{3.35}$, N124H$^{3.42}$, and T205M$^{5.54}$, do not reside in ligand-contacting positions, and, except for M117F$^{3.35}$, are at positions that are at least 10 Å away from the ligands in the β2ADR structures. These are proposed to trigger conformational changes leading to distinct G-protein activation (69).

8. Validation vs. experimental 3D structures

There are a few cases in which homology model-assisted binding-site prediction and site-directed mutagenesis could be evaluated in hindsight using experimental structures. For example, the structure of carazolol in complex with β2ADR is in line with earlier site-directed mutagenesis results supporting the involvement of the three polar residues D$^{3.32}$, S$^{5.42}$, and N$^{7.39}$ in binding of agonists and antagonists, and the spatial distribution of those three critical residues in a b-Rho-based homology model is quite close to the solved crystal structure (9). Recently, an important initiative involved a community-wide modeling and docking experiment *prior* to the release of the structure of A_{2A} adenosine receptor (86). The most accurate model in terms of ligand RMSD and correct contacts was selected and ranked on the basis of docking scores and agreement with available mutational data, interpreted on the basis of previous modeling studies by S. Costanzi (86).

A new GPCRdock experiment (http://gpcr.scripps.edu/GPCRDock2010/index.html) provided assessment of the current status of GPCR ligand-binding site modeling (87). GPCR-ligand complex details could be accurately predicted using closely related templates and incorporation of experimental data (87). These results are very encouraging in view of the constantly increasing numbers of available GPCR templates, as more and more Xray structures are being solved (88).

Acknowledgments

We thank the Niedersachsen-Israeli research foundation (M.Y.N.) and the German Research Foundation, Deutsche Forschungsgemeinschaft (ME1024/2-3) (W.M.) and (ME 2014/8-1) (W.M., M.B. and M.Y.N), for funding and Dr. Talia Yarnitzky and Dr. Merav Fichman for helpful comments.

References

1. Heilker R et al (2009) G-protein-coupled receptor-focused drug discovery using a target class platform approach. Drug Discov Today 14:231–240
2. Rosenbaum DM, Rasmussen SGF, Kobilka BK (2009) The structure and function of G-protein-coupled receptors. Nature 459: 356–363
3. Topiol S, Sabio M (2009) X-ray structure breakthroughs in the GPCR transmembrane region. Biochem Pharmacol 78:11–20
4. Sprang SR (2011) Cell signalling: binding the receptor at both ends. Nature 469:172–173
5. Xu F et al (2011) Structure of an agonist-bound human A2A adenosine receptor. Science 332(6027):322–327
6. Mobarec JC, Sanchez R, Filizola M (2009) Modern homology modeling of G-protein coupled receptors: which structural template to use? J Med Chem 52:5207–5216
7. Yarnitzky T, Levit A, Niv MY (2010) Homology modeling of G-protein-coupled receptors with X-ray structures on the rise. Curr Opin Drug Discov Devel 13:317–325
8. Senderowitz H, Marantz Y (2009) G Protein-coupled receptors: target-based in silico screening. Curr Pharm Des 15:4049–4068
9. de Graaf C, Rognan D (2009) Customizing G Protein-coupled receptor models for structure-based virtual screening. Curr Pharm Des 15: 4026–4048
10. Reisert J, Restrepo D (2009) Molecular tuning of odorant receptors and its implication for odor signal processing. Chem Senses 34: 535–545
11. Cui M et al (2006) The heterodimeric sweet taste receptor has multiple potential ligand binding sites. Curr Pharm Des 12:4591–4600
12. Brockhoff A et al (2010) Structural requirements of bitter taste receptor activation. Proc Natl Acad Sci U S A 107:11110–11115
13. Lagerstrom MC, Schioth HB (2008) Structural diversity of G protein-coupled receptors and significance for drug discovery. Nat Rev Drug Discov 7:339–357
14. Harmar AJ et al (2009) IUPHAR-DB: the IUPHAR database of G protein-coupled receptors and ion channels. Nucleic Acids Res 37:D680–D685
15. Petrel C et al (2004) Positive and negative allosteric modulators of the Ca^{2+}-sensing receptor interact within overlapping but not identical binding sites in the transmembrane domain. J Biol Chem 279:18990–18997
16. Bhattacharya S et al (2010) Allosteric antagonist binding sites in class B GPCRs: corticotropin receptor 1. J Comput Aided Mol Des 24:659–674
17. Niv MY et al (2006) Modeling activated states of GPCRs: the rhodopsin template. J Comput Aided Mol Des 20:437–448
18. Niv MY, Filizola M (2008) Influence of oligomerization on the dynamics of G-protein-coupled receptors as assessed by normal mode analysis. Proteins 71:575–586
19. Ivanov AA, Barak D, Jacobson KA (2009) Evaluation of homology modeling of G-protein-coupled receptors in light of the A(2A) adenosine receptor crystallographic structure. J Med Chem 52:3284–3292
20. Slack JP et al (2010) Modulation of bitter taste perception by a small molecule hTAS2R antagonist. Curr Biol 20:1104–1109
21. Biarnes X et al (2010) Insights into the binding of phenyltiocarbamide (PTC) agonist to its target human TAS2R38 bitter receptor. PLoS One 5:e12394
22. Vaidehi N, Pease JE, Horuk R (2009) Modeling small molecule-compound binding to G-protein-coupled receptors. Methods Enzymol 460:263–288
23. Simms J et al (2009) Homology modeling of GPCRs. Methods Mol Biol 552:97–113
24. Zhang Y (2009) I-TASSER: fully automated protein structure prediction in CASP8. Proteins 77(Suppl 9):100–113
25. Ballesteros JA, Weinstein H (1995) Integrated methods for the construction of three dimensional models and computational probing of structure function relations in G protein-coupled receptors. Methods Neurosci 25: 366–428
26. Okuno Y et al (2008) GLIDA: GPCR ligand database for chemical genomics drug discovery database and tools update. Nucleic Acids Res 36:D907–D912
27. Ivetac A, McCammon JA (2010) Mapping the druggable allosteric space of G-protein-coupled receptors: a fragment-based molecular dynamics approach. Chem Biol Drug Des 76:201–217
28. Beukers MW et al (1999) TinyGRAP database: a bioinformatics tool to mine G-protein-coupled receptor mutant data. Trends Pharmacol Sci 20:475–477
29. Horn F, Lau AL, Cohen FE (2004) Automated extraction of mutation data from the literature: application of MuteXt to G protein-coupled receptors and nuclear hormone receptors. Bioinformatics 20:557–568
30. Costanzi S (2008) On the applicability of GPCR homology models to computer-aided drug discovery: a comparison between in silico

and crystal structures of the beta2-adrenergic receptor. J Med Chem 51:2907–2914

31. Reynolds KA, Katritch V, Abagyan R (2009) Identifying conformational changes of the beta(2) adrenoceptor that enable accurate prediction of ligand/receptor interactions and screening for GPCR modulators. J Comput Aided Mol Des 23:273–288
32. Laurie AT, Jackson RM (2005) Q-SiteFinder: an energy-based method for the prediction of protein-ligand binding sites. Bioinformatics 21:1908–1916
33. Cherezov V et al (2007) High-resolution crystal structure of an engineered human beta2-adrenergic G protein-coupled receptor. Science 318:1258–1265
34. Hanson MA et al (2008) A specific cholesterol binding site is established by the 2.8 A structure of the human beta2-adrenergic receptor. Structure 16:897–905
35. Floriano WB et al (2006) Modeling the human PTC bitter-taste receptor interactions with bitter tastants. J Mol Model 12:931–941
36. Miguet L, Zhang Z, Grigorov MG (2006) Computational studies of ligand-receptor interactions in bitter taste receptors. J Recept Signal Transduct Res 26:611–630
37. Rasmussen SG et al (2011) Structure of a nanobody-stabilized active state of the beta(2) adrenoceptor. Nature 469:175–180
38. Horn F et al (2003) GPCRDB information system for G protein-coupled receptors. Nucleic Acids Res 31:294–297
39. Jones G et al (1997) Development and validation of a genetic algorithm for flexible docking. J Mol Biol 267:727–748
40. Friesner RA et al (2004) Glide: a new approach for rapid, accurate docking and scoring. 1. Method and assessment of docking accuracy. J Med Chem 47:1739–1749
41. Halgren TA et al (2004) Glide: a new approach for rapid, accurate docking and scoring. 2. Enrichment factors in database screening. J Med Chem 47:1750–1759
42. Venkatachalam CM et al (2003) LigandFit: a novel method for the shape-directed rapid docking of ligands to protein active sites. J Mol Graph Model 21:289–307
43. Wu G et al (2003) Detailed analysis of grid-based molecular docking: a case study of CDOCKER-A CHARMm-based MD docking algorithm. J Comput Chem 24:1549–1562
44. Wallace AC, Laskowski RA, Thornton JM (1995) LIGPLOT: a program to generate schematic diagrams of protein-ligand interactions. Protein Eng 8:127–134
45. Fang G et al (1999) PCR-mediated recombination: a general method applied to construct chimeric infectious molecular clones of plasma-derived HIV-1 RNA. Nat Med 5:239–242
46. Reichling C, Meyerhof W, Behrens M (2008) Functions of human bitter taste receptors depend on N-glycosylation. J Neurochem 106:1138–1148
47. Behrens M et al (2004) Molecular cloning and characterisation of DESC4, a new transmembrane serine protease. Cell Mol Life Sci 61:2866–2877
48. Cunningham BC, Wells JA (1989) High-resolution epitope mapping of hGH-receptor interactions by alanine-scanning mutagenesis. Science 244:1081–1085
49. Ueda T et al (2003) Functional interaction between T2R taste receptors and G-protein alpha subunits expressed in taste receptor cells. J Neurosci 23:7376–7380
50. Di Virgilio F, Steinberg TH, Silverstein SC (1990) Inhibition of Fura-2 sequestration and secretion with organic anion transport blockers. Cell Calcium 11:57–62
51. Bufe B et al (2002) The human TAS2R16 receptor mediates bitter taste in response to beta-glucopyranosides. Nat Genet 32:397–401
52. Behrens M et al (2004) The human taste receptor hTAS2R14 responds to a variety of different bitter compounds. Biochem Biophys Res Commun 319:479–485
53. Kuhn C et al (2004) Bitter taste receptors for saccharin and acesulfame K. J Neurosci 24:10260–10265
54. Sela I et al (2010) G protein coupled receptors-in silico drug discovery and design. Curr Top Med Chem 10:638–656
55. Brockhoff A et al (2007) Broad tuning of the human bitter taste receptor hTAS2R46 to various sesquiterpene lactones, clerodane and labdane diterpenoids, strychnine, and denatonium. J Agric Food Chem 55:6236–6243
56. de Graaf C et al (2008) Molecular modeling of the second extracellular loop of G-protein coupled receptors and its implication on structure-based virtual screening. Proteins 71:599–620
57. Shi L, Javitch JA (2004) The second extracellular loop of the dopamine D2 receptor lines the binding-site crevice. Proc Natl Acad Sci U S A 101:440–445
58. Mustafi D, Palczewski K (2009) Topology of class A G protein-coupled receptors: insights gained from crystal structures of rhodopsins, adrenergic and adenosine receptors. Mol Pharmacol 75:1–12
59. Bokoch MP et al (2010) Ligand-specific regulation of the extracellular surface of a G-protein-coupled receptor. Nature 463:108–112
60. Ahuja S et al (2009) Helix movement is coupled to displacement of the second extracellular

loop in rhodopsin activation. Nat Struct Mol Biol 16:168–175

61. Shi L, Javitch JA (2002) The binding site of aminergic G protein-coupled receptors: the transmembrane segments and second extracellular loop. Annu Rev Pharmacol Toxicol 42:437–467
62. Coetsee M et al (2008) Identification of Tyr(290(6.58)) of the human gonadotropin-releasing hormone (GnRH) receptor as a contact residue for both GnRH I and GnRH II: importance for high-affinity binding and receptor activation. Biochemistry 47:10305–10313
63. Pronin AN et al (2004) Identification of ligands for two human bitter T2R receptors. Chem Senses 29:583–593
64. Sakurai T et al (2010) Characterization of the beta-D-glucopyranoside binding site of the human bitter taste receptor hTAS2R16. J Biol Chem 285(36):28373–28378
65. Hall SE et al (2009) Elucidation of binding sites of dual antagonists in the human chemokine receptors CCR2 and CCR5. Mol Pharmacol 75:1325–1336
66. Wacker D et al (2010) Conserved binding mode of human beta2 adrenergic receptor inverse agonists and antagonist revealed by X-ray crystallography. J Am Chem Soc 132:11443–11445
67. Jaakola V-P et al (2008) The 2.6 Angstrom crystal structure of a human A2A adenosine receptor bound to an antagonist. Science 322:1211–1217
68. Goodwin JA et al (2007) Roof and floor of the muscarinic binding pocket: variations in the binding modes of orthosteric ligands. Mol Pharmacol 72:1484–1496
69. Rodriguez GJ et al (2010) Evolution-guided discovery and recoding of allosteric pathway specificity determinants in psychoactive bioamine receptors. Proc Natl Acad Sci U S A 107:7787–7792
70. Gloriam DE et al (2009) Definition of the G protein-coupled receptor transmembrane bundle binding pocket and calculation of receptor similarities for drug design. J Med Chem 52:4429–4442
71. Wu B et al (2010) Structures of the CXCR4 chemokine GPCR with small-molecule and cyclic peptide antagonists. Science 330: 1066–1071
72. Warne T et al (2011) The structural basis for agonist and partial agonist action on a beta(1)-adrenergic receptor. Nature 469:241–244
73. Chien EY et al (2010) Structure of the human dopamine D3 receptor in complex with a D2/D3 selective antagonist. Science 330:1091–1095
74. Jaakola VP et al (2010) Ligand binding and subtype selectivity of the human A(2A) adenosine receptor: identification and characterization of essential amino acid residues. J Biol Chem 285:13032–13044
75. Hofmann KP et al (2009) A G protein-coupled receptor at work: the rhodopsin model. Trends Biochem Sci 34:540–552
76. de Graaf C, Rognan D (2008) Selective structure-based virtual screening for full and partial agonists of the beta2 adrenergic receptor. J Med Chem 51:4978–4985
77. Vaidehi N (2010) Dynamics and flexibility of G-protein-coupled receptor conformations and their relevance to drug design. Drug Discov Today 15(21–22):951–957
78. Bhattacharya S, Vaidehi N (2010) Computational mapping of the conformational transitions in agonist selective pathways of a G-protein coupled receptor. J Am Chem Soc 132: 5205–5214
79. Provasi D, Filizola M (2010) Putative active states of a prototypic g-protein-coupled receptor from biased molecular dynamics. Biophys J 98:2347–2355
80. Ishikawa M et al (2010) Investigation of the histamine H3 receptor binding site. Design and synthesis of hybrid agonists with a lipophilic side chain. J Med Chem 53:6445–6456
81. Shapiro DA et al (2002) Evidence for a model of agonist-induced activation of 5-hydroxytryptamine 2A serotonin receptors that involves the disruption of a strong ionic interaction between helices 3 and 6. J Biol Chem 277:11441–11449
82. Jiang Q et al (1997) Mutagenesis reveals structure-activity parallels between human A2A adenosine receptors and biogenic amine G protein-coupled receptors. J Med Chem 40: 2588–2595
83. Kim J et al (1995) Site-directed mutagenesis identifies residues involved in ligand recognition in the human A2a adenosine receptor. J Biol Chem 270:13987–13997
84. Balaraman GS, Bhattacharya S, Vaidehi N (2010) Structural insights into conformational stability of wild-type and mutant beta1-adrenergic receptor. Biophys J 99:568–577
85. Hilser VJ (2010) An ensemble view of allostery. Science 327:653–654
86. Michino M et al (2009) Community-wide assessment of GPCR structure modelling and ligand docking: GPCR Dock 2008. Nat Rev Drug Discov 8:455–463
87. Kufareva I et al (2011) Status of GPCR modeling and docking as reflected by community-wide GPCR dock 2010 Assessment, *Structure* 19:1108–1126
88. Jacobson KA and Costanzi S (2012) New insights for drug design from the X-ray crystallographic structures of GPCRs. Mol Pharmacol doi:10.1124/mol.112.079335